Inorganic Chemistry

Article

pubs.acs.org/IC

Does Local Disorder Occur in the Pyrochlore Zirconates?

Peter E.R. Blanchard, Richard Clements, Brendan J. Kennedy,* Chris D. Ling, and Emily Reynolds

School of Chemistry, The University of Sydney, Sydney, NSW 2006 Australia

Max Avdeev, Anton P.J. Stampfl, and Zhaoming Zhang

Australian Nuclear Science and Technology Organisation, Lucas Heights, New South Wales 2234, Australia

Ling-Yun Jang

Facility Utilization Group, Experiment Facility Division, National Synchrotron Radiation Research Center, Hsinchu 30076, Taiwan

ABSTRACT: The zirconates $Ln_2Zr_2O_7$ (Ln = lanthanoid) have been studied using a combination of Zr L-edge X-ray absorption near edge structure (XANES) and synchrotron X-ray and neutron powder diffraction methods. These studies demonstrate that as the size of the lanthanoid cation decreases, the local structure evolves smoothly from the ideal pyrochlore toward the defect fluorite rather than undergoing an abrupt transformation. The Zr L-edge spectrum is found to be extremely sensitive to changes in the local coordination environment and demonstrates an increase in local disorder across the pyrochlore oxides. The sensitivity of the XANES measurements enables us to identify the progressive nature of the transition that could not be detected using bulk diffraction techniques.

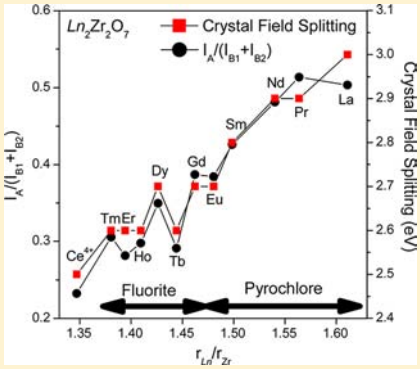

INTRODUCTION

Many metallic elements can be incorporated into the $A_2B_2O_7$ pyrochlore structure with a number of different oxidation state combinations observed, including A^+/B^{6+}, A^{2+}/B^{5+}, and A^{3+}/B^{4+}.[1] A number of the chemically distinct materials that adopt the pyrochlore structure display technologically important properties including catalytic activity, piezoelectricity, ferro- and ferrimagnetism, luminescence, and giant magnetoresistance.[1,2] The pyrochlore materials are also of interest for the immobilization of radioactive waste.[3,4] Lanthanoid zirconates, $Ln_2Zr_2O_7$, are being actively developed for use in thermal barrier coatings due to their low thermal conductivity, relatively high thermal expansion coefficient, and potentially high operating temperature. Their ionic conductivity is comparable to the industry standard yttria-stabilized zirconia (YSZ) electrolytes.[5−9] Consequently, substantial efforts are currently underway to develop these materials as thin films.[10−13]

The pyrochlore formula is best written as $A_2B_2X_6Y$, where A, B are cations and X, Y are anions. Most pyrochlore oxides (X = Y = oxygen) crystallize in the cubic space group $Fd\bar{3}m$ (No. 227). There are four possible choices of origin in this space group; the most commonly used places the smaller B-type cation at the 16*c* (0, 0, 0) site and the larger A-type cation at 16*d* (1/2, 1/2, 1/2). There are two occupied anion sites, with O (or *X*) at 48*f* (*x*, 1/8, 1/8), and O′ (or *Y*) at 8*b* (3/8, 3/8, 3/8). In this structure the cubic lattice parameter, *a*, and the positional parameter, *x*, for the O atom in 48*f* are the only structural variables. The pyrochlore structure is a 2 × 2 × 2 superstructure of fluorite (M_4X_8) in which the 8*a* (1/8, 1/8, 1/8) sites are vacant and there is an ordering of the two cations, Figure 1. The vacancy at the 8*a* site allows the surrounding anions to relax from the ideal position in fluorite, giving rise to an observable superstructure in the anionic array. The fluorite structure is in space group $Fm\bar{3}m$ where both the cations and

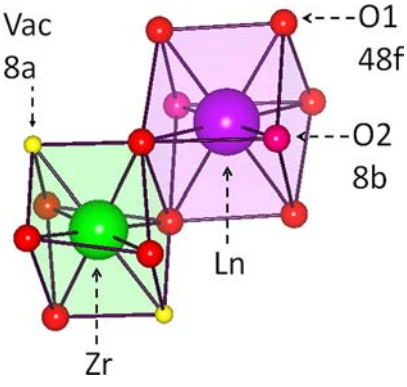

Figure 1. Representation of the pyrochlore structure showing the relationship to the fluorite structure. In the fluorite the 8*a* sites are fully occupied.

Received: July 31, 2012
Published: October 11, 2012

   dx.doi.org/10.1021/ic301677b | *Inorg. Chem.* 2012, 51, 13237−13244

Table 1. Atomic Positions and Atomic Displacement Parameters (10^{-3} Å^2) for $La_2Zr_2O_7$ Refined against Neutron Diffraction Data[a]

atom	position	x/a	y/b	z/c	U^{11}	$U^{22} = U^{33}$	$U^{12} = U^{13}$	U^{23}
La	16*d*	1/2	1/2	1/2	5.9(2)	5.9(2)	−0.8(3)	−0.8(3)
Zr	16*c*	0	0	0	4.0(2)	4.0(2)	1.3(3)	1.3(3)
O	48*f*	0.3313(1)	1/8	1/8	8.5(4)	5.4(3)	0	3.2(3)
O′	8*b*	3/8	3/8	3/8	5.7(4)	5.7(4)	0	0

[a] a = 10.78864(10) Å. R_p = 6.20%, R_{wp} = 8.00%, χ^2 = 1.85.

anions occupy special positions and the only variable structural parameter is the unit cell length. The lattice parameter of pyrochlores is 2a with respect to fluorite a_f (a ~5 Å).

The precise shapes of the cation polyhedra in the pyrochlore structure are dependent on value of the O 48*f* positional parameter, x.[14] The smaller B-type cation is coordinated to the six O-type anions in a distorted octahedron, and the larger A-type cation is in a distorted cube that is commonly described as a puckered six membered ring of O atoms with two O′ atoms forming linear O′−A−O′ chains, that are normal to the average plane of the six-membered ring.[1] The A−O and A−O′ bond distances are very different. The A−O′ bonds are among the shortest known for lanthanoid oxides (~2.2 Å) whereas the A−O distances are closer to the sum of the ionic radii of the two ions (~2.4−2.5 Å).[1] The interactions between the B_2O_6 and A_2O' sublattices in pyrochlore are relatively weak which allows the structure to tolerate a large degree of substitutional[15] as well as displacive disorder on the A-cation site.[16,17] Vacancies in the A_2O' sublattice are reasonably widespread, and even when there are no A-site vacancies the O′ anion site (8*b*) may not be fully occupied.[1]

The ordering of the two cations in the pyrochlore is driven, in part, by differences in their sizes and charges. In the lanthanoid zirconates, where the cation charges are fixed, the ratio of the Ln and Zr cation radii is the most accurate indicator of structure.[1] It is generally accepted that the ordered pyrochlore structure is favored when the lanthanoid radius is larger than Gd, and the smaller lanthanoids form defect fluorites.[1] Under some conditions, including high temperature, the Ln and Zr cations in a pyrochlore can become disordered over the A and B sites, and the anions are distributed over the 48*f*, 8*b* and the normally unoccupied 8*a* anion sites, each of these being partially occupied.[1] The order−disorder transition from the pyrochlore to the defect-fluorite structure is a very rare example of simultaneous disordering of both anions and cations.[18] Previous studies show that heating $Ln_2Zr_2O_7$ with Ln = Nd−Gd induces a pyrochlore−defect fluorite transition with the transition temperature rapidly decreasing as the ionic radii of the lanthanoid cation decreases: from 2300 °C in $Nd_2Zr_2O_7$ to 1530 °C in $Gd_2Zr_2O_7$.[19] Complex transformations can also occur upon the application of pressure.[20]

The phase transformation at high temperature may hinder the efficiency of these materials for use as electrolytes or thin films.[21,22] Chemical substitution can also induce a pyrochlore-defect fluorite phase transformation.[23−25] Glerup et al.[25] recently revisited the series $Y_2Ti_{2-x}Zr_xO_7$ first studied by Heremans et al.,[26] and described the presence of an intermediate disordered phase. Mandal et al.[27] on $Nd_{2-x}Y_yZr_xO_7$ and Whittle et al.[28] on La_{2-x} $Y_xZr_2O_7$ have provided evidence for disorder near the transition point. This was also clearly evident in neutron diffraction studies of the series $Nd_{2-x}Ho_xZr_2O_7$.[29] In this series the defect fluorite and pyrochlore phases are observed to coexist. The coexistence of these phases is not surprising given the need for simultaneous disordering of both anions and cations at the transition. However, traditional diffraction methods are not optimal for the study of such disorder. In the present work the feasibility of using X-ray absorption near edge structure (XANES) to probe the local structure in oxides of the type $Ln_2Zr_2O_7$ is examined. While XANES has been previously used to study disorder in gadolinium-based pyrochlores ($Gd_2Zr_2O_7$, $Gd_2Ti_{2-x}Zr_xO_7$) near the pyrochlore-defect fluorite phase boundary,[30,31] a comprehensive study of the rare-earth zirconates $Ln_2Zr_2O_7$ has not been completed. The aim is to first establish whether or not disorder is evident in XANES measurements, particularly in Zr L_3-edge XANES measurements, and second to determine the extent of this disorder. Surprisingly, the spectral changes indicate that disorder is endemic in the entire Zr pyrochlore series.

EXPERIMENTAL SECTION

Synthesis. Oxides of the type $Ln_2Zr_2O_7$ (Ln = lanthanoid La−Tm except Pm) were prepared using conventional solid-state methods. Stoichiometric quantities of the appropriate lanthanoid oxide and ZrO_2 (calcined at 1000 °C overnight before use), sufficient to prepare ~20 g of material, were finely mixed before being fired at 1200 °C for 24 h. The resulting powders were then reground, under acetone, for 10 min before being heated at 1450 °C for 85 h. This process was repeated as necessary to yield single-phase samples as established using a Panalytical X'Pert Pro X-ray diffractometer.

Diffraction Measurements. Synchrotron X-ray powder diffraction (S-XRD) data were collected at ambient temperature in the angular range 5° < 2θ < 85°, using X-rays of wavelength 0.825 18 Å on the powder diffractometer at BL-10 of the Australian Synchrotron.[32] The sample was placed in a 0.3 mm diameter capillary that was rotated during the measurements. Neutron powder diffraction (NPD) data were obtained over the angular range 10° < 2θ < 160° using the high-resolution powder diffractometer Echidna at ANSTO's OPAL facility at Lucas Heights, Australia.[33] The wavelength of the incident neutrons was either 1.492 Å (La sample, Ge(335) reflection, takeoff angle 120°) or 1.300 Å (all the other samples, Ge(337) reflection, takeoff angle 140°). For these measurements the samples were contained in 12 mm diameter vanadium cans.

Structures were refined using the Rietveld method implemented in the program Rietica.[34] The neutron peak shape was modeled using a pseudo-Voigt function convoluted from asymmetry resulting from axial divergence, and the background was estimated using a fourth-order polynomial in 2θ, which was refined simultaneously with the other profile and structural parameters. Anisotropic atomic displacement parameters (ADPs) were refined as allowed by symmetry. These refinement results are summarized in Table 1. The peak shape in the synchrotron data was modeled using a pseudo-Voigt function, and the background was estimated using a linear interpolation between a set of 40 background points.

Zr and Ce L_3-edge XANES. The Zr and Ce L_3-edge XANES spectra were collected on beamline 16A1 at the National Synchrotron Radiation Research Center (NSRRC) in Hsinchu, Taiwan.[35] Finely ground samples were dispersed onto Kapton tape and placed in front of the X-ray beam at a 45° angle. Spectra were collected in fluorescence yield mode using a Lytle detector. An energy step-size

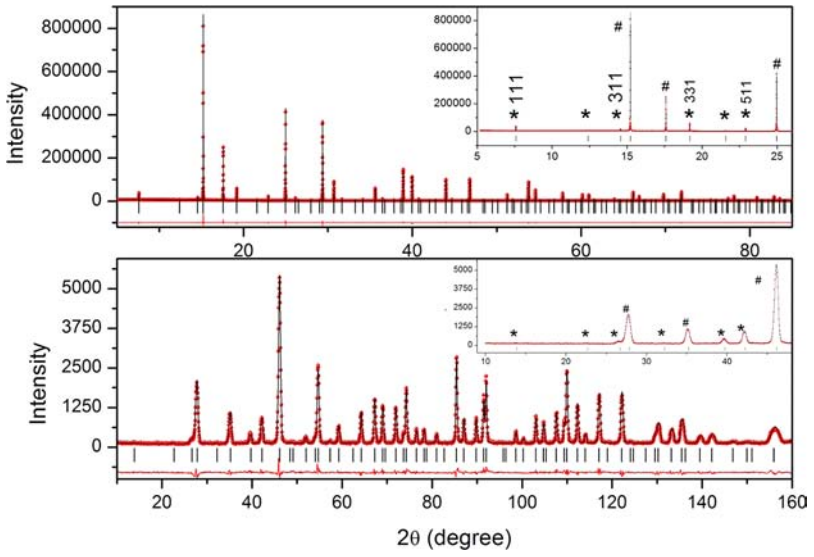

Figure 2. Synchrotron X-ray λ = 0.825 18 Å (upper) and neutron λ = 1.492 Å (lower) powder diffraction profiles for $La_2Zr_2O_7$. The solid lines are the result of the Rietveld analysis. The insets illustrate the presence of the low-angle superlattice reflections indicative of the pyrochlore lattice that are marked with *. Only those reflections marked # would be observed for a defect fluorite structure.

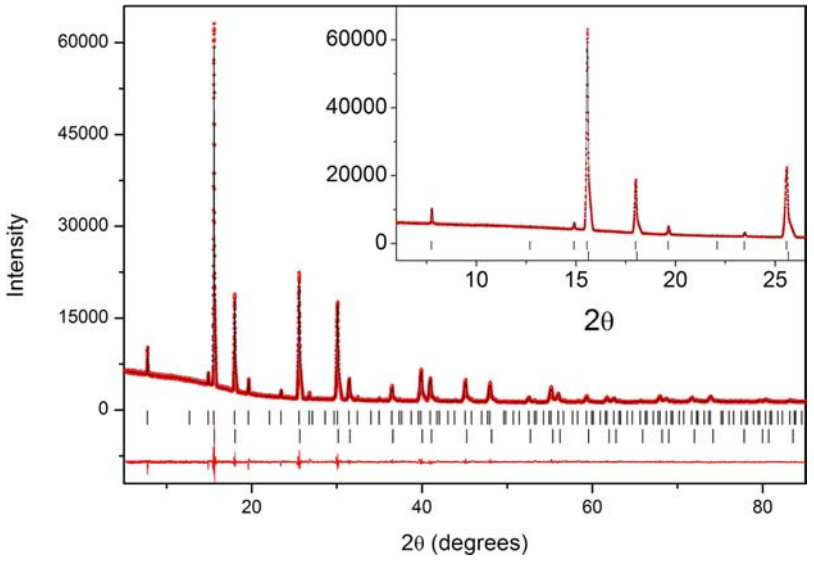

Figure 3. Synchrotron X-ray (λ = 0.825 18 Å) diffraction profiles for $Gd_2Zr_2O_7$. The solid lines are the result of the Rietveld analysis. The diffraction data showed the presence of some poorly crystalline defect fluorite material, as indicated by the lower set of Bragg reflections. The inset demonstrates the presence of superlattice reflections indicative of the pyrochlore lattice and the broadening of the reflections.

of 0.2 eV was used near the absorption edge. The Zr L_3-edge spectra were calibrated against elemental Zr with the maximum in the first derivative of the L_3-edge set to 2222.3 eV. The Ce L_3-edge spectra were calibrated against elemental Cr with the maximum in the first derivative of the K-edge set to 5989.2 eV. All XANES spectra were analyzed using the Athena software program.[36]

RESULTS AND DISCUSSION

1. Diffraction. The X-ray diffraction profile for $La_2Zr_2O_7$ illustrated in Figure 2 contains a number of weak reflections indicative of cation and/or anion-vacancy ordering demonstrating that a pyrochlore type structure in space group $Fd\bar{3}m$ is formed. The strongest of these have hkl = (111), (311), and (331). That these peaks are weak can be explained by considering that the X-ray contrast between La^{3+} (Z = 57) and Zr^{4+} (Z = 40) is modest and that the anion-vacancy ordering only involves the O′ anion on the 8*b* sites and not the six O anions on the 48*f* sites. Stronger superlattice reflections are evident in the neutron pattern (Figure 2), reflecting the greater relative sensitivity of neutron diffraction to light elements in the presence of heavy atoms such as La or Zr. The X-ray and neutron profiles for $Nd_2Zr_2O_7$ (not shown) are similar to those displayed in Figure 2, and there is no doubt that the average structure for this material is that of a pyrochlore. Unfortunately it is not practical to measure neutron diffraction patterns for the oxides with Ln = Sm, Eu, or Gd due to their high neutron absorption cross sections. A recent neutron diffraction study of $Gd_2Zr_2O_7$ that employed Gd-160 demonstrated this compound to be a pyrochlore.[37] The synchrotron diffraction patterns for the three oxides $Ln_2Zr_2O_7$ (Ln = Sm, Eu, and Gd) all contained superlattice reflections indicative of the pyrochlore structure. In the present work the synchrotron X-ray diffraction peaks of the pyrochlore

dx.doi.org/10.1021/ic301677b | Inorg. Chem. 2012, 51, 13237−13244

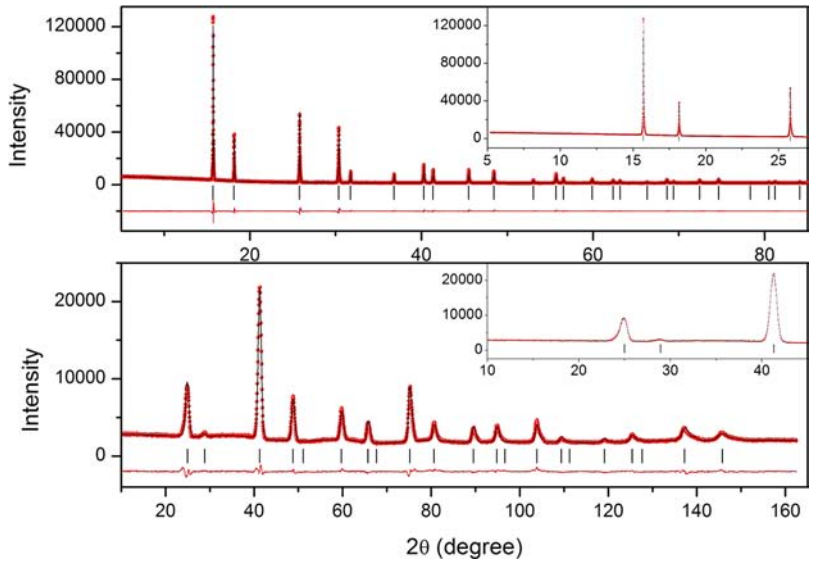

Figure 4. Synchrotron X-ray λ = 0.825 18 Å (upper) and neutron λ = 1.300 Å (lower) powder diffraction profiles for $Tb_2Zr_2O_7$. The solid lines are the result of the Rietveld analysis. The insets demonstrate the absence of any superlattice reflections indicative of the pyrochlore lattice demonstrating the structure to be defect fluorite.

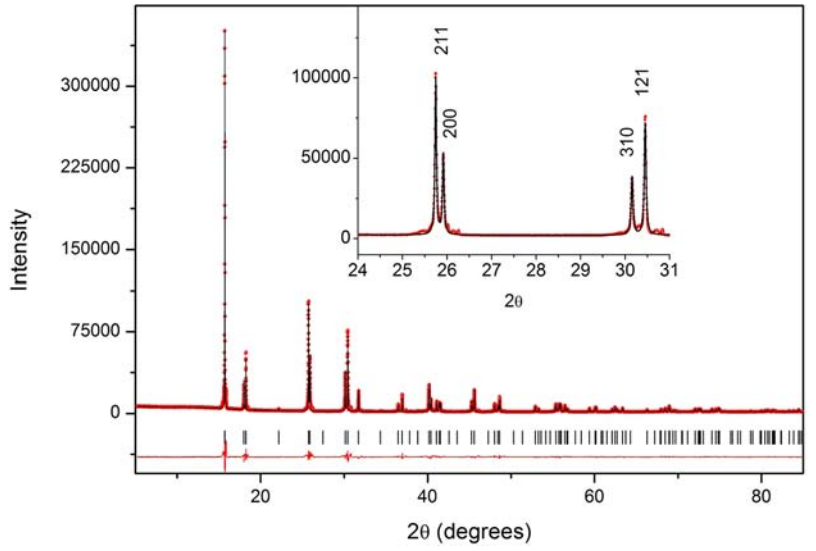

Figure 5. Synchrotron X-ray (λ = 0.825 18 Å) diffraction profiles for $Ce_{0.5}Zr_{0.5}O_2$. The solid lines are the result of the Rietveld analysis. The inset demonstrates the effect of the tetragonal distortion with the $(220)_F$ peak appearing as a (211)/(200) doublet, and the $(311)_F$ peak as a (310)/(121) doublet.

phase in $Gd_2Zr_2O_7$ are somewhat broader than those for either $La_2Zr_2O_7$ or $Nd_2Zr_2O_7$; for example, the strongest reflection (222) (near 2θ = 15.5°) had a full width at half-maximum of 0.097° in $Gd_2Zr_2O_7$ compared to 0.016° for Ln = La or 0.022° for Ln = Nd. The half-width of the corresponding (111) reflection in the defect fluorite $Tb_2Zr_2O_7$ ($Tb_{0.5}Zr_{0.5}O_{1.75}$) is 0.038°. In addition the asymmetry of the fundamental reflections in the synchrotron pattern provides evidence for the presence of some defect fluorite-type material in $Gd_2Zr_2O_7$ (see Figure 3). There was no evidence for superlattice reflections indicative of the pyrochlore structure in the synchrotron diffraction pattern of $Tb_2Zr_2O_7$.

Rietveld refinements of the structures of $La_2Zr_2O_7$ and $Nd_2Zr_2O_7$ against the neutron diffraction data confirmed that the space group $Fd\bar{3}m$ is appropriate. Anisotropic ADPs were employed in these refinements, and selected values are listed in Table 1. The refined structure shows large anisotropic displacements of the A-site cations and 48*f* O anions that are consistent with their local symmetry. Tabira et al.[38] have found structured features in the selected area electron diffraction patterns for $La_2Zr_2O_7$ showing that such displacements are correlated on a small scale. The presence (or absence) of such displacive disorder in no way invalidates the description of $La_2Zr_2O_7$ and $Nd_2Zr_2O_7$ as an ordered pyrochlore.

In comparison, the X-ray profile of $Tb_2Zr_2O_7$ (Figure 4) shows no evidence for any superlattice reflections characteristic of the pyrochlore structure type, nor were such reflections observed in the neutron profile. The structure is, therefore, best described as a defect fluorite with formula $Tb_{0.5}Zr_{0.5}O_{1.75}$. A strong modulation of the background is apparent in the neutron profile indicating short-range correlations arising from the presence of local oxygen vacancy and/or cation ordering.

dx.doi.org/10.1021/ic301677b | *Inorg. Chem.* 2012, 51, 13237−13244

Similar modulation was evident in the neutron profile of the related oxide $La_2Ce_2O_7$ that also has a defect fluorite structure.[39]

In summary, the diffraction data reinforce the widespread view that a cubic pyrochlore structure forms for Ln with ionic radii larger than that of Gd, while the defect fluorite structure forms for smaller lanthanoids. It is important for the reader to note that the samples are highly crystalline and that, with the exception of $Gd_2Zr_2O_7$, there is no justification from either the X-ray or (when available) neutron diffraction profiles to argue that long-range disorder is present in those oxides adopting pyrochlore structures.

As part of this work we attempted to prepare the corresponding Ce-containing zirconate "$Ce_2Zr_2O_7$". The X-ray diffraction pattern of this sample (Figure 5) demonstrates that we in fact obtained the tetragonal fluorite $Ce_{0.5}Zr_{0.5}O_2$ and the synchrotron profile for this material was well fitted in the $P4_2/nmc$ space group (Table 2). In this structure, Ce and Zr are

Table 2. Atomic Positions and ADPs (10^{-3} Å^2) for $Ce_{0.5}Zr_{0.5}O_2$ Refined against Synchrotron Diffraction Data in Space Group $P42/nmc$[a]

atom	position	x/a	y/b	z/c	U_{iso}
Ce/Zr	8*e*	3/4	1/4	3/4	7.5(1)
O	16*h*	1/4	1/4	0.4608(8)	13.9(8)

[a] a = 3.68080(5), c = 5.27380(7) Å. R_p = 7.62%, R_{wp} = 12.56%.

disordered on the 8*e* sites, and each is coordinated to eight oxygen anions, with four nearest neighbors at 2.148(2) Å and four more distant at 2.393(3) Å. The local coordination environment of the Zr in $Ce_{0.5}Zr_{0.5}O_2$ is therefore different from that in either the pyrochlore or defect fluorite structure.

2. Zr L_3-Edge X-ray Absorption Spectra. The Zr L_3-edge XANES spectra of several $Ln_2Zr_2O_7$ zirconates are shown in Figure 6a. The L_3-edge corresponds to the dipole-allowed

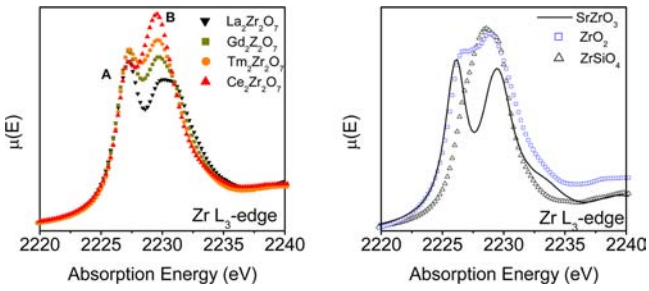

Figure 6. (a) Zr L_3-edge XANES spectra of $La_2Zr_2O_7$, "$Ce_2Zr_2O_7$", $Gd_2Zr_2O_7$, and $Tm_2Zr_2O_7$. (b) Zr L_3-edge XANES spectra of 6-coordinate ($SrZrO_3$), 7-coordinate (ZrO_2), and 8-coordinate ($ZrSiO_4$) Zr standards. All spectra were collected in fluorescence mode.

transition of $2p_{3/2}$ electrons into unoccupied 4d states. As these are the states that are directly involved in bonding, information on the coordination environment of the Zr cations can be obtained from the line shape. In general, two features (labeled A and B) are observed in all Zr L_3-edge XANES spectra: see Figure 6 for examples. In 6-coordinate systems, features A and B corresponds to the t_{2g} and e_g states, respectively.[40] The energy levels of t_{2g} and e_g states are reversed in 8-coordinate cubic systems. Surprisingly, when compared to standards of known coordination environments (Figure 6b), the zirconates have a different line shape from the 6-coordinate ($SrZrO_3$) or 8-coordinate ($ZrSiO_4$) standards. For the pyrochlore phases, feature B is broader than that of $SrZrO_3$ with a shoulder toward higher absorption energy, similar to that observed in the Ti L-edge of 6-coordinated Ti systems, including $Gd_2Ti_2O_7$.[31,41,42] In 6-coordinate systems, the e_g states are more sensitive to distortions of the local structure due to the overlap of d_{z^2} and $d_{x^2-y^2}$ states with ligand states, and such distortions result in broadening of the corresponding XANES spectral features.[41] Peak-broadening caused by local distortion has been previously observed in $Pb(Zr_{1-x}Ti_x)O_3$.[43] The lineshapes of the defect fluorite phases are more similar to those of ZrO_2 (7-coordinate) than to those of $ZrSiO_4$. The defect fluorites here are actually anion-deficient with 7/8th of the O sites occupied. Therefore, the Zr coordination number (CN) is closer to 7 than 8, and in this case, none of the metal d-orbitals point directly toward the ligand orbitals. The crystal symmetry may also influence the line shape of the Zr L_3-edge,[44] although this influence is expected to be minimal compared to the effect of changes in the local environment.

Further information on the coordination environment of Zr was obtained by fitting the experimental Zr L_3-edge XANES spectra to component peaks. There are several different methods for fitting XANES spectra.[40,44−47] As shown in Figure 7, spectra were fitted to Gaussian peaks with the edge-jump fitted to a single arc-tan function.[44] Feature A was fitted to a single peak (labeled A). There is very little change in the width of this peak across the lanthanoid series, likely due to a similar degree of hybridization of the O 2p states with t_{2g} states in pyrochlores and e_g states in defect fluorites. Feature B was fitted to two peaks (labeled B1 and B2) to account for peak broadening across the series. In general, B2 becomes less intense relative to B1 progressing from the pyrochlore to the fluorite. A similar trend was also observed in the Ti L_3-edge of $Gd_2Ti_{2-x}Zr_xO_7$ pyrochlores where the e_g peak became more symmetrical with Zr substitution.[31] Such disorder would decrease the tetragonal distortion in the TiO_6 octahedrons. This would effectively introduce more disorder around the Ti atoms.[31] The change in the shape of feature B of the Zr L_3-edge across the rare-earth series can be also attributed to a similar increase in disorder around the Zr atoms in the pyrochlore oxides.

Across the series, with the exception of "$Ce_2Zr_2O_7$" which will be discussed further below, several trends are evident from the fitted spectra. Figure 8 shows a plot of the crystal field splitting (ΔE) as a function of the radius ratio (r_{Ln}/r_{Zr}). The crystal field splitting, taken as the energy difference between peaks A and B1, can be used to qualitatively determine changes in the Zr coordination number (CN).[31,40,48] Surprisingly, a general decrease in ΔE is observed across the pyrochlore phases approaching the pyrochlore-defect fluorite phase boundary, indicating an increase in the CN of Zr atoms. In contrast, ΔE across the defect fluorite phases does not change much, indicating that the CN remains the same. The value for the Tb compound appears anomalous, and this may reflect partial oxidation to Tb^{4+}. A similar trend is observed in the intensity ratio of feature A to feature B ($I_A/(I_{B1} + I_{B2})$), where a decrease in $I_A/(I_{B1} + I_{B2})$ as a function of Ln size is more noticeable in the pyrochlores than the defect fluorites (Figure 8). Such trends were not observed in the Ti-L studies of $Gd_2Ti_{2-x}Zr_xO_7$,[31] suggesting that disorder alone cannot explain the changes in the Zr L_3-edge line shape across the rare-earth series. Both trends support the conclusion that, within the pyrochlore phases the average Zr CN increases as the size of the lanthanoid cation

dx.doi.org/10.1021/ic301677b | Inorg. Chem. 2012, 51, 13237−13244

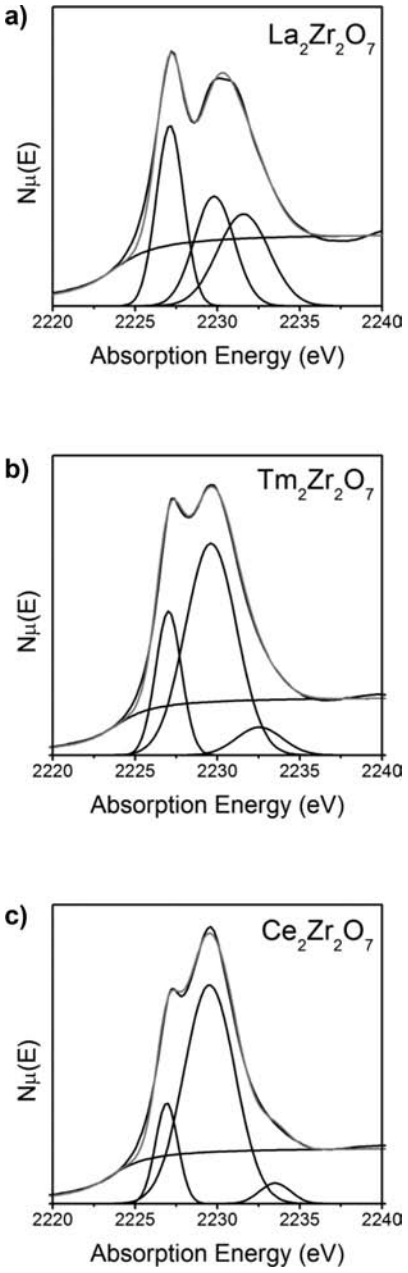

Figure 7. Fitted XANES spectra of (a) $La_2Zr_2O_7$, (b) $Tm_2Zr_2O_7$, and (c) "$Ce_2Zr_2O_7$".

decreases. However, once the defect fluorite phase is formed, the changes are much smaller, suggesting minimal change in the CN of Zr.

The above observation raises questions about the nature of order and disorder in the pyrochlore and fluorite zirconates. An increase in the CN of Zr suggests an increase in disorder throughout the pyrochlore zirconates, either by the migration of oxygen from 48*f* and 8*b* sites to the unoccupied 8*a* site or by the creation of cation antisites, where the Zr^{4+} cations partially occupy the A-site, displacing Ln^{3+} cations to the octahedral sites. As described above, the current neutron and synchrotron diffraction measurements are consistent with published work and show no evidence for long-range disorder in the pyrochlores.[30,37] This is not entirely surprising given that traditional neutron and synchrotron diffraction techniques that only consider the Bragg reflections are not necessarily sensitive

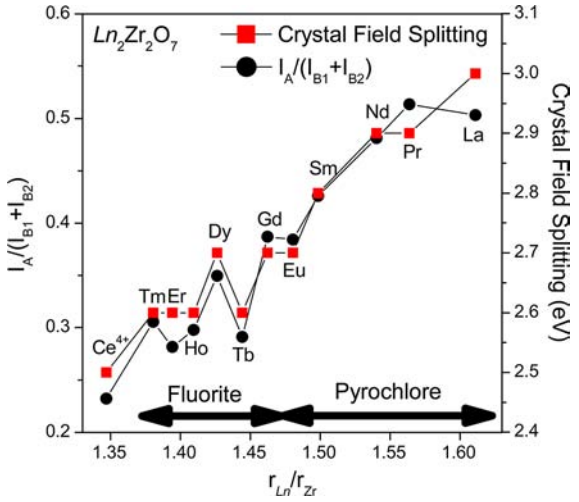

Figure 8. Plots of the crystal field splitting (ΔE) and the intensity ratio of features A and B ($I_A/(I_{B1} + I_{B2})$) as a function of r_{Ln}/r_{Zr}. Peak intensities are taken as the area of the peaks.

to local distortions within an ordered crystal structure. Total scattering methods are more sensitive to local distortions. X-ray absorption spectroscopy, Raman spectroscopy, and nuclear magnetic resonance have been used previously to measure local distortion in several titanate and molybdenum pyrochlores that was not observed in diffraction and scattering experiments.[48−50] Our XANES analysis shows that local disorder is present in the pyrochlore phases and that this increases as the lanthanoid size decreases until the fully disordered defect fluorite phase forms. XANES proved to be a powerful technique for analyzing the local structure of these materials, providing evidence of local distortion that was not detected from diffraction measurements.

Returning now to "$Ce_2Zr_2O_7$" that diffraction demonstrated to be tetragonal fluorite $Ce_{0.5}Zr_{0.5}O_2$. That the Ce is present as Ce^{4+} in this sample was confirmed by examination of the Ce L_3-edge XANES spectrum (Figure 9). The Ce L-edge is highly sensitive to the oxidation state of Ce.[51] Three peaks are observed in the Ce L_3-edge spectra (labeled A, B, and C). Peaks A−C correspond to the $4f^0$, $4f^1L^1$, and $4f^2L^2$ final states (*L* denotes a ligand hole), respectively.[52] When compared to $CeAlO_3$ (Ce^{3+}) and CeO_2 (Ce^{4+}), the line shape is nearly

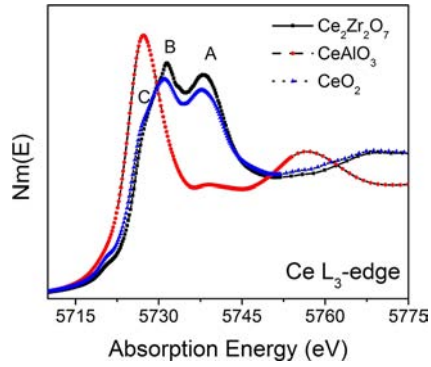

Figure 9. Ce L_3-edge XANES spectra, collected in fluorescence mode, of "$Ce_2Zr_2O_7$", $CeAlO_3$, and CeO_2. Peaks A−C correspond to the $4f^0$, $4f^1L^1$, and $4f^2L^2$ final states (*L* denotes a ligand hole), respectively, and are characteristic of Ce^{4+}.[52] The absorption energies and intensities of peaks A−C are approximately the same in both "$Ce_2Zr_2O_7$" and CeO_2, reflecting similar covalent character and coordination environments.[53].

dx.doi.org/10.1021/ic301677b | *Inorg. Chem.* 2012, 51, 13237−13244

identical to that of CeO_2, indicating that Ce^{3+} in "$Ce_2Zr_2O_7$" has been completely oxidized to Ce^{4+} (i.e., the molecular formula should be written as $Ce_{0.5}Zr_{0.5}O_2$).

The line shape of the Zr L_3-edge of "$Ce_2Zr_2O_7$" ($Ce_{0.5}Zr_{0.5}O_2$) (Figure 6a) is considerably different from those of the Zr-containing pyrochlores or defect fluorites described above; feature B was much more intense than feature A for $Ce_{0.5}Zr_{0.5}O_2$. Such a line shape is similar to that observed in the Ce-rich region of the CeO_2−ZrO_2 phase diagram.[52] The intensity ratio and crystal field splitting of $Ce_{0.5}Zr_{0.5}O_2$ (Figure 8) suggests that the Zr CN is higher than that of the other zirconates. The higher CN indicates that Zr atoms are surrounded by more O atoms than in the other zirconates. This is consistent with the bulk structural studies that show the Zr in $Ce_{0.5}Zr_{0.5}O_2$ to be eight-coordinated, whereas in the defect fluorites the Zr is effectively seven-coordinated. The excess O is stabilized by a change in the oxidation state of Ce^{3+}, as confirmed from the Ce L_3-edge XANES analysis (Figure 9). This is a powerful illustration of the sensitivity of the Zr L_3-edge to local coordination and suggests it is possible to distinguish between oxygen deficient and stoichiometry Zr fluorites.

CONCLUSIONS

In conclusion, we have demonstrated, using Zr L-edge XANES data, that local disorder occurs right across the $Ln_2Zr_2O_7$ series. Two important messages come from this work. First, bulk diffraction methods can provide evidence for long-range anion disorder, although X-ray diffraction methods are of limited value. As evidenced by the recent study of $Nd_{1-x}Ho_xZr_2O_7$, neutron methods are more suitable for detecting anion disorder.[29] Second, the Zr L-edge spectrum is extremely sensitive to changes in the local coordination environment. This sensitivity enables us to identify the evolutionary nature of the pyrochlore-defect fluorite transition that could not be detected using synchrotron or laboratory-based X-ray diffraction techniques. Finally, given that XANES can easily be a surface sensitive technique by detecting electron yields, the methodology used here to study the local structure of bulk zirconates could easily be extended to thin film samples being investigated for use as electrolytes or thermal barrier coatings.

AUTHOR INFORMATION

Corresponding Author

*E-mail: b.kennedy@chem.usyd.edu.au.

Notes

The authors declare no competing financial interest.

ACKNOWLEDGMENTS

This work was, in part, performed at the powder diffraction beamline at the Australian Synchrotron with the assistance of Dr. Helen Brand. We acknowledge the support of the Australian Research Council for this work. The work performed at the NSRRC was supported by the Australian Synchrotron International Access Program.

REFERENCES

(1) Subramanian, M. A.; Aravamudan, G.; Rao, G. V. S. *Prog. Solid State Chem.* **1983**, *15*, 55−143.
(2) Weller, M. T.; Hughes, R. W.; Rooke, J.; Knee, C. S.; Reading, J. *Dalton Trans.* **2004**, 3032−3041.
(3) Ewing, R. C.; Weber, W. J.; Lian, J. *J. Appl. Phys.* **2004**, *95*, 5949−5971.
(4) Lian, J.; Helean, K. B.; Kennedy, B. J.; Wang, L. M.; Navrotsky, A.; Ewing, R. C. *J. Phys. Chem. B* **2006**, *110*, 2343−2350.
(5) Hagiwara, T.; Yamamura, H.; Nishino, H. *J. Fuel Cell Sci. Technol.* **2011**, *8*, 051020.
(6) Feng, J.; Xiao, B.; Wan, C. L.; Qu, Z. X.; Huang, Z. C.; Chen, J. C.; Zhou, R.; Pan, W. *Acta Mater.* **2011**, *59*, 1742−1760.
(7) Cao, X. Q. *J. Mater. Sci. Technol.* **2007**, *23*, 15−35.
(8) Guillaume, M.; Fischer, P.; Roessli, B.; Allenspach, P.; Trounov, V. *Physica C* **1994**, *235*, 1637−1638.
(9) Brett, D. J. L.; Atkinson, A.; Brandon, N. P.; Skinner, S. J. *Chem. Soc. Rev.* **2008**, *37*, 1568−1578.
(10) Chen, H. S.; Kumar, R. V.; Glowacki, B. A. *Mater. Chem. Phys.* **2010**, *122*, 305−310.
(11) Roche, V.; Jimenez, C.; Chaudouet, P.; Benaboud, R.; Weiss, F.; Sarigiannidou, E. *Thin Solid Films* **2012**, *520*, 2566−2574.
(12) Yu, Z. M.; Odier, P.; Morlens, S.; Chaudouet, P.; Bacia, M.; Zhou, L.; Zhang, P. X.; Jin, L. H.; Li, C. S.; David, P.; Fruchart, O.; Lu, Y. F. *J. Sol-Gel Sci. Technol.* **2010**, *54*, 363−370.
(13) Kim, J. W.; Jeong, G. E.; Yang, H. S. *Phys. Status Solidi A* **2011**, *208*, 1105−1110.
(14) Kennedy, B. J.; Hunter, B. A.; Howard, C. J. *J. Solid State Chem.* **1997**, *130*, 58−65.
(15) Knee, C. S.; Rainford, B. D.; Weller, M. T. *J. Mater. Chem.* **2000**, *10*, 2445−2447.
(16) Li, L. Q.; Kennedy, B. J. *Chem. Mater.* **2003**, *15*, 4060−4067.
(17) Somphon, W.; Ting, V.; Liu, Y.; Withers, R. L.; Zhou, Q.; Kennedy, B. J. *J. Solid State Chem.* **2006**, *179*, 2495−2505.
(18) Champion, J. D. M.; Wills, A. S.; Fennell, T.; Bramwell, S. T.; Gardner, J. S.; Green, M. A. *Phys. Rev. B* **2001**, *64*, 140407.
(19) Michel, D.; Perez y Jorba, M.; Collongues, R. *Mater. Res. Bull.* **1974**, *9*, 1457−1468.
(20) Zhang, F. X.; Lang, M.; Liu, Z. X.; Ewing, R. C. *Phys. Rev. Lett.* **2010**, *105*, 015503.
(21) Gupta, T. K.; Lange, F. F.; Bechtold, J. H. *J. Mater. Sci.* **1978**, *13*, 1464−1470.
(22) Ma, W.; Gong, S. K.; Xu, H. B.; Cao, X. Q. *Surf. Coat. Technol.* **2006**, *200*, 5113−5118.
(23) Radhakrishnan, A. N.; Rao, P. P.; Sibi, K. S.; Deepa, M.; Koshy, P. *J. Solid State Chem.* **2009**, *182*, 2312−2318.
(24) Liu, Y.; Withers, R. L.; Noren, L. *J. Solid State Chem.* **2004**, *177*, 4404−4412.
(25) Glerup, M.; Nielsen, O. F.; Poulsen, F. W. *J. Solid State Chem.* **2001**, *160*, 25−32.
(26) Heremans, C.; Wuensch, B. J.; Stalick, J. K.; Prince, E. *J. Solid State Chem.* **1995**, *117*, 108−121.
(27) Mandal, B. P.; Krishna, P. S. R.; Tyagi, A. K. *J. Solid State Chem.* **2010**, *183*, 41−45.
(28) Whittle, K. R.; Cranswick, L. M. D.; Redfern, S. A. T.; Swainson, I. P.; Lumpkin, G. R. *J. Solid State Chem.* **2009**, *182*, 442−450.
(29) Clements, R.; Avdeev, M.; Hester, J. R.; Kennedy, B. J.; Ling, C. D.; Stampfl, A. P. J. *J. Solid State Chem.* **2011**, *184*, 2108−2213.
(30) Lee, Y. H.; Chen, J. M.; Lee, J. F.; Kao, H. C. I. *J. Chin. Chem. Soc.* **2009**, *56*, 543−548.
(31) Nachimuthu, P.; Thevuthasan, S.; Adams, E. M.; Weber, W. J.; Begg, B. D.; Mun, B. S.; Shuh, D. K.; Lindle, D. W.; Gullikson, E. M.; Perera, R. C. C. *J. Phys. Chem. B* **2005**, *109*, 1337−1339.
(32) Wallwork, K. S.; Kennedy, B. J.; Wang, D. *AIP Conf. Proc.* **2007**, *879*, 879−882.
(33) van Dijk, M. P.; Burggraaf, A. J.; Cormack, A. N.; Catlow, C. R. A. *Solid State Ionics* **1985**, *17*, 159−167.
(34) Hunter, B. A.; Howard, C. J. *RIETICA A Computer Program for Rietveld Analysis of X-Ray and Neutron Powder Diffraction Patterns*; 1998.
(35) Dann, T. E.; Chung, S. C.; Huang, L. J.; Juang, J. M.; Chen, C. I.; Tsang, K. L. *J. Synchrotron Radiat.* **1998**, *5*, 664−666.
(36) Ravel, B.; Newville, M. *J. Synchrotron Radiat.* **2005**, *12*, 537−541.
(37) Kennedy, B. J.; Zhou, Q. D.; Avdeev, M. *J. Solid State Chem.* **2011**, *184*, 1695−1698.

(38) Tabira, Y.; Withers, R. L.; Yamada, T.; Ishizawa, N. *Z. Kristallogr.* **2001**, *216*, 92−98.
(39) Reynolds, E.; Blanchard, P. E. R.; Zhou, Q. D.; Kennedy, B. J.; Zhang, Z. M.; Jang, L. Y. *Phys. Rev. B* **2012**, *85*, 132101.
(40) Galoisy, L.; Pelegrin, E.; Arrio, M. A.; Ildefonse, P.; Calas, G. *J. Am. Ceram. Soc.* **1999**, *82*, 2219−2224.
(41) Schneller, T.; Kohlstedt, H.; Petraru, A.; Waser, R.; Guo, J.; Denlinger, J.; Learmonth, T.; Glans, P. A.; Smith, K. E. *J. Sol-Gel Sci. Technol.* **2008**, *48*, 239−252.
(42) Henderson, G. S.; Liu, X.; Fleet, M. E. *Phys. Chem. Miner.* **2002**, *29*, 32−42.
(43) Ray, S. C.; Hsueh, H. C.; Wu, C. H.; Pao, C. W.; Asokan, K.; Liu, M. T.; Tsai, H. M.; Chuang, C. H.; Pong, W. F.; Chiou, J. W.; Tsai, M. H.; Lee, J. M.; Jang, L. Y.; Chen, J. M.; Lee, J. F. *Appl. Phys. Lett.* **2011**, *99*, 042909.
(44) Zhang, F.; Chupas, P. J.; Lui, S. L. A.; Hanson, J. C.; Caliebe, W. A.; Lee, P. L.; Chan, S. W. *Chem. Mater.* **2007**, *19*, 3118−3126.
(45) Chen, C. L.; Dong, C. L.; Rao, S. M.; Chern, G.; Chen, M. C.; Wu, M. K.; Chang, C. L. *J. Phys.: Condens. Matter* **2008**, *20*, 255236.
(46) Nachimuthu, P.; Shih, W. C.; Liu, R. S.; Jang, L. Y.; Chen, J. M. *J. Solid State Chem.* **2000**, *149*, 408−413.
(47) Rakovan, J.; Newville, M.; Sutton, S. *Am. Mineral.* **2001**, *86*, 697−700.
(48) Lummen, T. T. A.; Handayani, I. P.; Donker, M. C.; Fausti, D.; Dhalenne, G.; Berthet, P.; Revcolevschi, A.; van Loosdrecht, P. H. M. *Phys. Rev. B* **2008**, *77*, 214310.
(49) Booth, C. H.; Gardner, J. S.; Kwei, G. H.; Heffner, R. H.; Bridges, F.; Subramanian, M. A. *Phys. Rev. B* **2000**, *62*, R755−R758.
(50) Keren, A.; Gardner, J. S. *Phys. Rev. Lett.* **2001**, *87*, 177201.
(51) Zhang, Z. M.; Kennedy, B. J.; Howard, C. J.; Jang, L. Y.; Knight, K. S.; Matsuda, M.; Miyake, M. *J. Phys.: Condens. Matter* **2010**, *22*, 445401.
(52) Kotani, A.; Kvashnina, K. O.; Butorin, S. M.; Glatzel, P. *J. Electron Spectrosc. Relat. Phenom.* **2011**, *184*, 210−215.
(53) Zhou, Q. D.; Blanchard, P.; Kennedy, B. J.; Reynolds, E.; Zhang, Z. M.; Miiller, W.; Aitken, J. B.; Avdeev, M.; Jang, L. Y.; Kimpton, J. A. *Chem. Mater.* **2012**, *24*, 2978−2986.